ACS Photonics
Article
pubs.acs.org/journal/apchd5

Spectral Tuning of Localized Surface Phonon Polariton Resonators for Low-Loss Mid-IR Applications

Yiguo Chen,[†,‡,§] Yan Francescato,[†,‡] Joshua D. Caldwell,[∥] Vincenzo Giannini,[‡] Tobias W. W. Maß,[⊥] Orest J. Glembocki,[∥] Francisco J. Bezares,[∥] Thomas Taubner,[⊥] Richard Kasica,[#] Minghui Hong,[§] and Stefan A. Maier*[,‡]

[‡]The Blackett Laboratory, Imperial College London, London SW7 2AZ, United Kingdom
[§]Department of Electrical and Computer Engineering, National University of Singapore, Singapore
[∥]U.S. Naval Research Laboratory, Washington, DC, United States
[⊥]RWTH Aachen University, Aachen, Germany
[#]National Institute of Standards and Technology, Gaithersburg, Maryland, United States

S *Supporting Information*

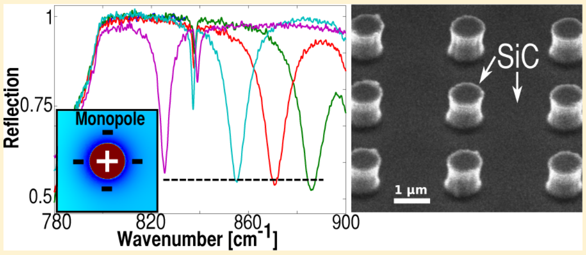

ABSTRACT: Low-loss surface phonon polariton (SPhP) modes supported within polar dielectric crystals are a promising alternative to conventional, metal-based plasmonic systems for the realization of nanophotonic components. Here we show that monopolar excitations in 4H-silicon carbide nanopillar arrays exhibit an unprecedented stable efficiency even when the resonator filling fraction is varied by an order of magnitude. This provides a powerful mid-IR platform with excellent spectral tunability and strong field confinement. Combining IR spectroscopy measurements with full electrodynamic calculations, we elucidate the nature of the optical modes in these elongated subwavelength nanostructures by investigating their spectral behavior and local field dependence on the size and periodicity. The present study also gives a clear understanding and practical guidelines for the spectral tuning of localized SPhP and the coupling mechanisms at play. This work is integral with the development of phonon-polariton based applications for surface-enhanced infrared absorption spectroscopy (SEIRA), polychromatic detectors, and thermal imaging.

KEYWORDS: *localized surface phonon polariton, monopolar resonance, silicon carbide, spectral tuning, near-field coupling*

Plasmonics offers a promising route to realize nanophotonic devices and is one of the predominant and most researched methods to achieve subdiffraction confinement of electromagnetic waves. This occurs through the coherent excitations of conduction electrons, or plasmons, in metallic nanostructures.[1] Unfortunately, the intrinsic optical losses associated with the fast scattering lifetimes of plasmons pose an inevitable limitation on the performance of metals.[2−4] Recently, much effort has been devoted to identifying low-loss alternative materials. For example, transparent conducting oxides[2] and the high-carrier-mobility graphene[5] have attracted enormous attention. Though improvements in the optical losses have been demonstrated using these materials, the performance is still expected to be mitigated by the Ohmic nature of their free carriers. In the mid-, far-infrared, and THz spectral regions, polar dielectric crystals have been identified as a potential low-loss alternative to metal-based plasmonics due to their ability to support surface phonon polariton (SPhP) modes.[6−11] In particular, silicon carbide (SiC) exhibits markedly reductions in the optical losses over metals in a frequency region (797−973 cm^{-1}), which is rich in molecular vibrations and thermal phenomena. This has led to its use in various SPhP and thermal schemes[6−8,12−18] as well as metamaterial designs.[19−21] Furthermore, the phonon-based nature of the subdiffraction confinement inherently introduces interesting potential deviations from the standard understanding of plasmonic systems, for instance, the reductions in the correlation lengths of the optical modes from SPhPs recently being shown in hexagonal boron nitride with thicknesses less than 1 nm.[11] Therefore, while analogous to the plasmonic phenomena, it is unclear whether the prior knowledge based on plasmonics could provide good descriptions of SPhP modes.

In an effort to develop some of this understanding, we present a detailed study of the modes supported by cylindrical nanopillars fabricated into a 4H-SiC substrate and their corresponding spectral behaviors upon changes in nanopillar diameter and interpillar gaps. SiC nanopillar arrays with diameters of 0.5, 0.75, and 1 μm are investigated using Fourier transform infrared (FTIR) spectroscopy at varied interpillar gaps. In contrast to a previous study,[7] we report here on the anomalous behavior of one type of mode, the monopole, that

Received: April 30, 2014
Published: July 3, 2014

exhibits a nearly constant intensity while shifting spectrally by over 60 cm^{-1} with the varied interpillar gaps. This constant intensity is achieved despite the filling fraction of the nanopillars being changed by over an order of magnitude. Using finite-element method (FEM) calculations, the different natures of all the observed modes are revealed, providing insights into the anomalous response of monopoles to the changing periodicity, the corresponding changes in the transverse dipoles, and elucidating as well the observed distinct trends in spectral shifts within both square and rectangular unit cell arrays. While there has been significant effort in investigating the interaction of light with plasmonic metal nanoparticles,[22−28] few studies have been reported on localized SPhP resonators as of yet.[7,8,21,29−31] Moreover, the presence of the underlying continuous SiC substrate in the nanostructures discussed here enables the stimulation of monopolar resonant modes rarely studied thus far.[7,32,33] Finally, similar to the efforts on plasmonic systems, the knowledge of the periodicity-induced spectral tuning and coupling mechanisms are crucial for understanding the basic physics by which such nanostructures interact with light. This work serves as practical guidelines for the future design of SiC SPhP architectures for mid-IR nanophotonics, thermal applications, and metamaterials.

■ GENERAL FEATURES OF LOCALIZED SPHP IN SIC NANOPILLARS

The SPhP modes excited in 4H-SiC are stimulated within the frequency window bound by the transverse optical phonon (TO) at 797 cm^{-1} (12.5 μm) and the longitudinal optical phonons (LO) at 973 cm^{-1} (10.3 μm),[34] referred as Reststrahlen band.[9,35,36] As shown in Figure 1a, the stimulation of optical phonons within the Reststrahlen band of polar dielectric crystals, which correspond to charged lattice oscillations, induces a negative permittivity leading to a dramatic increase in reflectivity (see inset in Figure 1a). Outside of this band, polar dielectrics behave as a typical, transparent dielectric material mainly defined by its index of refraction $n^2 \sim \mathcal{R}(\varepsilon)$. Within the Reststrahlen band, SiC (and polar dielectrics in general) can confine incident light to subdiffraction dimensions analogous to conventional plasmonic materials. However, due to the absence of free carriers, the scattering of the optical phonons occurs on a time scale of picoseconds, which is orders of magnitude longer than the scattering of free carriers in metals. This results in exceptionally small values of the imaginary part of the permittivity, leading to a subdiffraction confinement with low optical losses and high field enhancement.

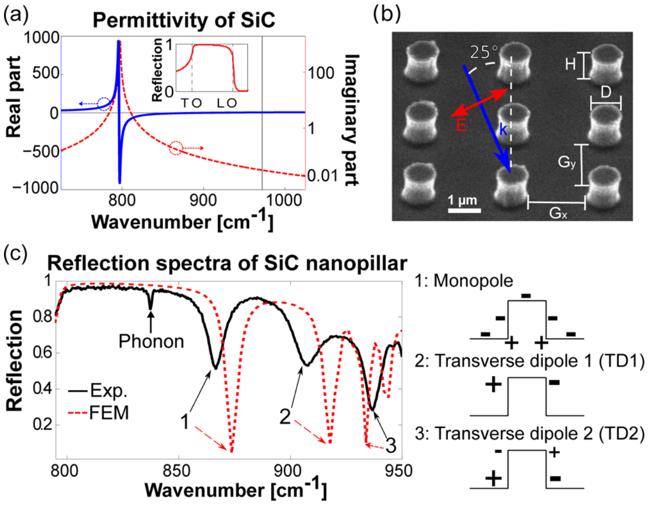

Figure 1. (a) Real (blue) and imaginary (red, in log scale) parts of the permittivity of 4H-SiC around its Reststrahlen band. The thin vertical line marks the change of sign of $\mathcal{R}\{\varepsilon\}$ and the LO position. The inset shows the reflectivity of a plain SiC substrate. (b) SEM image of the SiC pillar structure highlighting the geometric parameters where the gap $G = G_x = G_y$ in the case of square lattices. (c) Experimental (black solid) and FEM (red dashed curve) reflection spectra of 1 μm diameter and 1 μm high SiC nanopillars on a square lattice with a 2 μm interpillar gap. The dip marked out at 838 cm^{-1} in the experimental spectrum is a LO phonon which is only observed in nanopatterned SiC. Schematic charge configurations of the three modes are shown on the right-hand side.

A SEM image of a representative nanostructure used for this work is presented in Figure 1b. Note that the nanopillars and the substrate are of the same material, and the height $H = 1$ μm is used for all the samples. The infrared reflection spectra were collected using a Bruker Infinion microscope with a 15× Cassegrain objective, which illuminates the sample with a weighted average incident angle of 25°. Finite-element-method calculations were performed using commercial COMSOL multiphysics software with the permittivities derived from a 4H-SiC wafer. A p-polarized plane wave is launched within the xz-plane at an incident angle of 25° in the simulation to approximate the experimental conditions. A typical pair of reflection spectra from the experiment and FEM calculation are shown in Figure 1c with a diameter $D = 1$ μm and an interpillar gap $G = 2$ μm. The differences between the experimental and simulated spectra can be ascribed to the idealization of the geometry and excitation source within the simulation in comparison to the inherent structural variations and the additional induced surface damage resulting from the reactive-ion etching process during the experiment. The presence of the homogeneous negative-permittivity SiC substrate enables the stimulation of monopolar modes, which typically cannot couple to incident light due to the absence of charge neutrality. This mode can be regarded as a modified longitudinal dipolar mode with charge neutrality being provided by the negative-permittivity substrate and can therefore be stimulated by an out-of-plane electric field.[7,32,33,37,38] Apart from the monopolar mode, two transverse dipolar modes (TD1 and TD2) are excited by the in-plane electric field, analogous to the modes found in its plasmonic counterparts.[7,39,40] Small dips can also be noted in the FEM spectra, for example, on the blue (higher energy) side of TD2 (~944 cm^{-1}) in Figure 1c. These rather weak modes are the joint results of the dispersive permittivity around the LO phonon and the artificial chamfers introduced at the top and bottom of the nanopillars in the simulation; therefore, they are excluded from the discussion. Note that the modes are associated with peaks in the extinction, that is, $1 - R$, so that they appear as dips in the reflection spectra. More generally, the presented SiC resonators differ notably from their plasmonic counterparts because their deeply subwavelength character (down to $\lambda/100$)[7,10] allows the design of nanodevices for a 10−12.5 μm wavelength, giving rise to very high modal confinement, particularly appealing for surface-enhanced spectroscopy. This is reinforced by the extremely narrow modal line widths associated with long-lived state where the field amplification proceeds for many optical cycles.

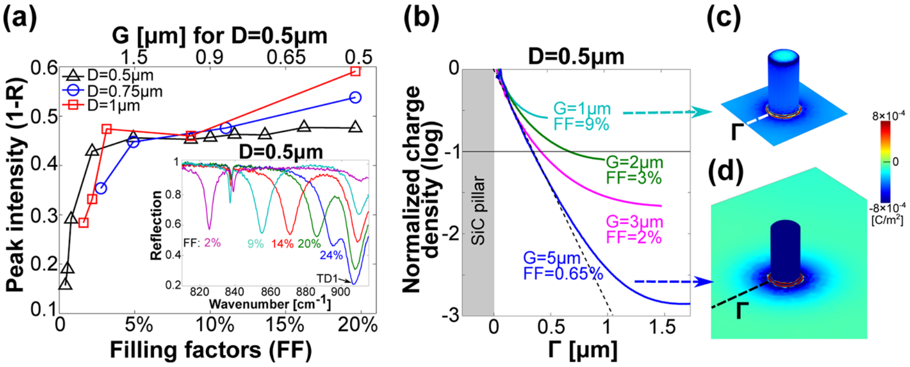

Figure 2. (a) Intensities of the monopoles calculated by $1 - \mathcal{R}$ at the peaks of the experimental spectra as a function of the filling factors. The inset shows the representative spectra from the samples with diameter $D = 0.5$ μm, presenting a nearly constant magnitude. The fractions under the monopoles are the corresponding FFs. (b) The normalized charge density in log scale as a function of the distance away from the edge of the pillars in the radial direction. Samples with $D = 0.5$ μm and FF of 9, 3, 2, and 0.65% are used as examples. (c, d) Corresponding 3D charge density distributions of FF = 9 and 0.65%, respectively. The interpillar region in (c) is covered by charge totally, while an isolated charge area can be identified in (d).

RESULTS AND DISCUSSION

Monopolar Spectral Tuning with Constant Efficiency. As discussed above, the occurrence of the negative permittivity within both the nanopillars and the underlying SiC substrate results in the observation of monopoles. These modes exhibit the anomalous behavior of a constant modal efficiency and broad-range spectral tuning with changing gap sizes. To explore this phenomenon, nanopillars arranged in a square lattice with diameters $D = 0.5$, 0.75, and 1 μm and varied interpillar gaps were fabricated. Figure 2a shows the monopolar resonance intensity with respect to the nanopillar filling fraction (FF), which is defined by $\pi D^2/4\Lambda^2$, with $\Lambda = G + D$ and the interpillar gap $G = G_x = G_y$. The peak intensity is defined by $1 - \mathcal{R}$ (taking into account the baseline).

Sharp changes in the intensity are observed at small FF (<5%), however, the modal amplitude becomes nearly constant for larger FF and remains so with increasing FF. This phenomenon coincides with a spectral shift of the monopole toward higher energy, until the mode merges with TD1 making its identification difficult. For the case of $D = 0.5$ μm, it is seen that over an order of magnitude difference in the nanopillar FF (2% < FF < 20%) leads to a significant spectral shift (>60 cm^{-1}) while leaving the mode extinction constant at about 45% (see the inset of Figure 2a, and monopoles that are spectrally close to the TD1, such as FF = 24%, are not considered, as the two modes may interact with each other). This indicates that, unlike previously explored plasmonic nanostructures,[24,28] spectrally tuning of the SPhP monopole can be induced by simple variations of the FF without the detrimental effect on the magnitude of the mode. In contrast, TD1 (see inset of Figure 2a) exhibits a progressive reduction in intensity with increasing gap (decreasing FF), as one would intuitively expect from a plasmonic system. This remarkable behavior of the monopoles coupled with high Q-factors ranging from 40−266, which correspond to line widths between 3 and 20 cm^{-1}, can be a huge advantage over the conventional plasmonic systems with a geometry-dependent efficiency, in applications such as polychromatic detectors, where constant efficiency is preferred.

The origin of such an anomalous dependence on the resonator FF stems from the effective charged area surrounding the pillar caused by the charge neutrality requirements of the stimulated monopole. To illustrate this, the calculated charge density distributions in the radial direction from the nanopillar base are studied. Four samples with $D = 0.5$ μm and FF = 9, 3, 2, and 0.65% are considered in Figure 2b, with the curves presenting the normalized charge density from the edge of the pillars to the middle of the gaps. The charge density exponentially decays first in the vicinity of the pillars, then saturates at different values based on the FF or the corresponding gap size. The point that this value drops by 1/*e* (marked by the horizontal line at −1 in log scale) is defined as the boundary of the charged area. The charged area extending beyond the nanopillar can cover in some cases as much as the entire interpillar region, as can be seen in Figure 2c. It appears that, as long as the charged region extends across the entire interpillar gap, the intensity of the monopole is maintained near its maximum value, which is demonstrated by the constant part in Figure 2a with FF > 5%. However, if the pillars are separated further, the resonators begin to act like isolated antennas as demonstrated in Figure 2d and the modal amplitude becomes proportional to FF as would ordinarily be anticipated (more information on the charge density is also presented in Figure S1). This can be easily explained by the following. Suppose S denotes the effective charged area governed by the monopole and $\Lambda = G + D$ represents the lattice constant, the resonance intensity a can be roughly estimated as $a \propto S/\Lambda^2$. When FF < 5%, $S \lesssim \Lambda^2$, a decreases as Λ increases in the typical, expected fashion. However, when FF $\gtrsim$ 5%, the charge density available to the monopole is limited by the size of the unit cell, which makes $S = \Lambda^2$ and, thus, a become constant.

Let us now explore further the near-fields of this mode. Detailed spatial distributions of the charge density and electric fields of the monopole for the case with a diameter $D = 1$ μm and gap $G = 2$ μm are presented in Figure 3 for illustration. The charges oscillating along the pillar and on the substrate in its vicinity are counterbalanced by the charges of the opposite sign on a ring at the bottom of the nanopillar, as shown in Figure 3a. This is also depicted in the cross section of E_z below the substrate surface ($z = -5$ nm) shown in Figure 3b. Further measurements confirmed the out-of-plane oscillating nature of monopoles as they exhibit enhanced extinctions under grazing incidence illumination as compared to 25° incident light (not shown). The charge distribution is rotationally symmetric around the central axis of the pillar despite the *p*-polarized light incident at off-normal angle, which causes the electric field distributions in the *xz* and *yz* cross sections to be nearly

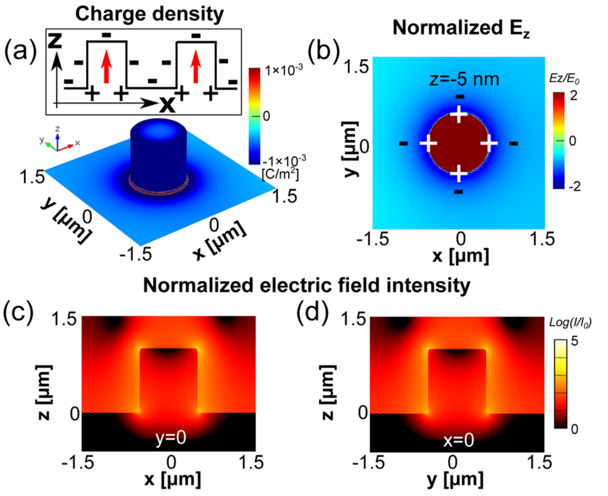

Figure 3. (a) 3D view of the charge distribution for the monopole mode. The inset shows the schematic charge configurations of two neighboring pillars for this mode, with "+" and "−" denoting the charges and red arrows showing the electric field direction. (b) Normalized E_z in the xy plane at −5 nm below the surface of the substrate. Please note the color is saturated in order to show the sign flip of E_z. (c, d) Normalized electric intensities in the planes $y = 0$ and $x = 0$, respectively. Note that these two cross sections are extremely similar to each other, despite the fact that the incident field is p-polarized in the xz plane. The charge density and E_z distributions are in linear scale and the electric field intensities are shown in log scale.

identical, as shown in Figure 3c,d. In addition, since the charge is well distributed around the pillar, the electric field enhancement can be observed across the whole sample, extending from the pillar to the entire gap region in some cases.

Spectral Behavior. *Size and Interpillar Gap Dependence in a Square Lattice.* Changes in the nanostructure geometry are a common and convenient tool to finely tune the spectral features of an optical system. Apart from the constant intensities of the monopoles, we continue the discussions of the spectral shifts of the various modes observed in the nanopillar arrays arranged in a square lattice with varied interpillar gaps and diameters D = 0.5, 0.75, and 1 μm. Reflection spectra from the samples with a diameter D = 1 μm are shown in Figure 4a to demonstrate the evolutions of the monopole, TD1 and TD2 with changing interpillar gap. The spectra of randomly arranged nanopillar arrays of the same diameters (see Figure S2 for a SEM image of such sample) are plotted against their periodic counterparts, which are related by FF. Good agreement between spectra collected from arrays featuring random and periodic arrangements of the nanopillars rules out the influence of diffractive coupling. Therefore, the coupling proceeds only through near-field interactions (overlap of adjacent evanescent fields). The spectra for D = 0.5 and 0.75 μm are plotted in Figure S3 of the Supporting Information.

In general, the monopole is coincident with TD1 at small gaps G and therefore cannot be identified, as is apparent in Figure 4a for the 1 μm diameter nanopillars with G < 1 μm. It then separates from TD1 and continues red-shifting as G increases. In contrast, the two dipolar modes blue-shift over a small frequency range with increasing G, consistent with plasmonic dipoles. To better illustrate their spectral behaviors, the respective resonance positions of all three modes are plotted as a function of G in Figure 4b−d for all three diameters. The opposite trends between monopole and TDs as well as the distinct variations in gap at which spectral shifts occur for the various modes suggest different near-field coupling mechanisms in these two kinds of modes.

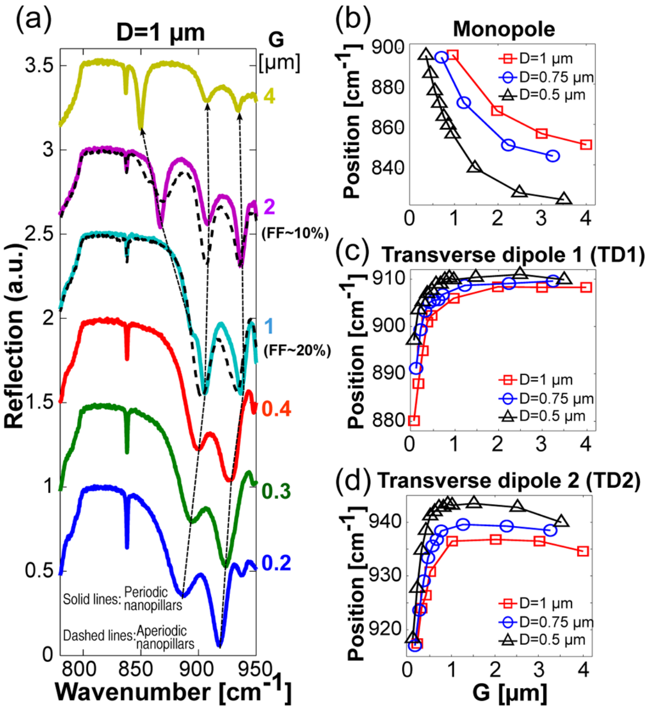

Figure 4. (a) Evolution of the experimental reflection spectra of the nanopillar arrays in square lattices as the interpillar gap size changes for a diameter D = 1 μm. Experimental spectral positions for the (b) monopole, (c) TD1, and (d) TD2 as a function of the interpillar gap size G. Black triangles, blue circles and red squares denote the data for a diameter D = 0.5, 0.75, and 1 μm, respectively.

This inverse dependence on gap size of the monopole and TDs can be explained using plasmonic hybridization theory[22,27,41,42] by referring to their near-field distributions. For the cases of monopoles (see inset of Figure 3a), the oscillating charges along the nanopillars are of the same sign. Decreasing the interpillar gap translates into an increased coulomb repulsion, thus these modes shift to higher energy. For TDs, the charges change sign across the diameter along the x-axis, as shown in Figure 5a and b, respectively. A "+ − + −" charge distribution is observed within neighboring nanopillars, as shown in the insets of Figure 5a,b. This in turn will lead to a decreased coulomb repulsion with reductions in interpillar gaps thereby shifting these resonances to lower frequencies.

More generally, the TDs supported by the elongated geometry of the nanopillars are expected to be found between the two limiting cases of $\mathcal{R}\{\varepsilon\} = -2$ (the Fröhlich condition for a sphere) and $\mathcal{R}\{\varepsilon\} = -1$ (the Fröhlich condition for an infinitely long cylinder).[40] TD1, with charge oscillations concentrated mainly near the tip of the nanopillar (Figure 5a) can be found roughly around $\mathcal{R}\{\varepsilon\} = -2$. This is consistent with experimental FTIR spectra collected prior to the removal of the metal hard mask used in the RIE process, where this metal mask on top of the pillar extinguished TD1 (see Figure S4 in the Supporting Information). TD2, with a near-field confined to the lower half of the nanopillar can be observed around $\mathcal{R}\{\varepsilon\} = -1$. This mode is not simply a higher order of TD1, its presence is due to the low losses associated with SiC. As it is not observed within higher-loss plasmonic systems, it

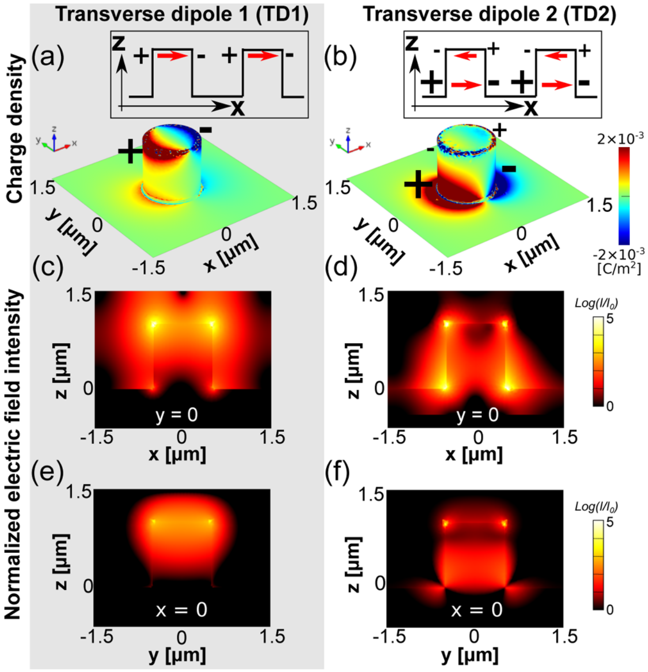

Figure 5. (a, b) 3D views of the charge density of the TD1 and TD2, respectively. The insets show schematic charge configurations of two neighboring pillars in the polarization plane for the corresponding modes, with "+" and "−" denoting the charges and red arrows showing the electric field direction. (c, d) Normalized electric field intensity in the $x = 0$ plane for the TD1 and TD2, respectively, and (e, f) in the $y = 0$ plane. The charge density distributions are in linear scale and the electric field intensities are shown in log scale.

has rarely been studied. Because these two TDs are located close to the aforementioned Fröhlich conditions, the spectral shift due to the retardation that can be induced is rather limited, as clearly observed in Figure 4c,d.

The electric fields are more intense in the interpillar region for the monopoles (Figure 3c,d) than the two TDs (Figure 5c−f). This also explains the observations from Figure 4b−d that TDs approach their stable spectral positions at considerably smaller gap sizes compared to monopoles, implying that the near-field coupling occurs only in very close vicinity of the nanopillars. While the near-field enhancement is slightly greater for the two TDs compared with that of the monopole, the spatial location of the near-field maximum at either the top or base of the nanopillar for TD1 and TD2 is not favorable practically speaking for some applications such as enhanced molecular spectroscopy. On the contrary, monopole is more attractive since its field localization is well distributed, covering the whole patterned surface and interpillar region and providing 10^3 field enhancement over μm^2 areas.

Interpillar Gap Dependence in a Rectangular Lattice. The distinct charge distributions of the monopole and TDs lead to distinct near-fields of these modes. From Figure 3c,d, it can be seen that despite the incident polarization being in the *xz*-plane, the near-field profile in the cross-section at $x = 0$ is almost identical to the cross-section at $y = 0$ for the monopole due to the uniform charge distribution around the nanopillars. In contrast, one can see in Figure 5c−f a large difference in near-field between these two orientations for the TDs as a result of in-plane charge oscillations. In order to probe the directionality of the near fields and the corresponding coupling effects, SiC nanopillar arrays in rectangular lattices were also fabricated.

Without loss of generality, we focus on SiC nanopillars with diameters $D = 1\ \mu m$. The interpillar gap in the *y*-axis (G_y) is fixed at 0.2 μm, while the gap size along (G_x) is varied from 0.2 to 4 μm. Two orthogonal incident planes, namely, *xz* and *yz*, are considered for each sample as illustrated in the schematic drawings in Figure 6a and b, respectively. In both cases, the light is *p*-polarized with an incident angle of 25°, similar to the above sections. The relative spectral shifts for the monopole, TD1, and TD2 observed in the experiment and simulation are plotted in Figure 6c−e. Note that we use the spectral position from the sample with $G_x = 4\ \mu m$ as reference for the monopole and that with $G_x = 0.2\ \mu m$ for TDs so that the relative spectral shifts are all positive in sign.

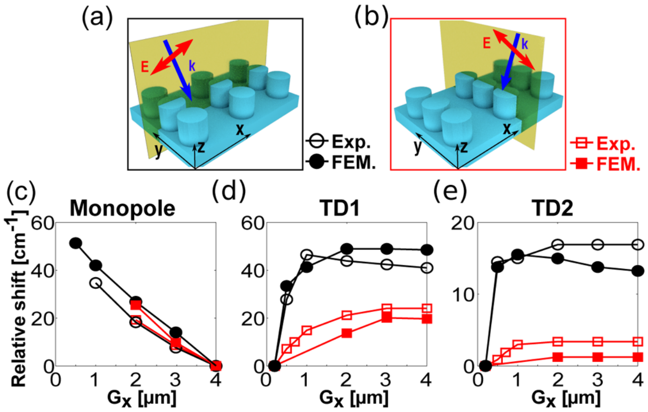

Figure 6. (a, b) SiC nanopillar arrays in rectangular lattices illuminated by *p*-polarized light in the *xz* and *yz* planes, respectively. The gap in the *y* direction is fixed at 0.2 μm, and the gap along the *x* direction is varied from 0.1 to 4 μm. (c, d, and e) Experimental and FEM relative spectral shifts of the monopole, TD1, and TD2, respectively. Data from the *xz* and *yz* incident planes are marked by the black circles and red squares, respectively.

From Figure 6c, one can recognize the highly overlapped trends of relative shifts for the monopoles under the two different planes of incidence. This incident-plane insensitivity is consistent with the near fields shown in Figure 3c,d. For TD1 and TD2 as shown in Figure 6d,e, the plots for both the experiment and FEM simulation reveal a larger shift when the in-plane polarization is aligned along the varied-gap direction (configuration in Figure 6a) compared with the orthogonal orientation (configuration in Figure 6b). This suggests that TD1 and TD2 are more sensitive to the interpillar gap size in the same direction as the transverse component of the incident light. This is confirmed by the fact that these modes, excited by the in-plane electric field component, have a stronger field distribution in the incident plane, as shown in Figure 5c,e.

■ CONCLUSIONS

We have demonstrated that SiC nanopillars attached to a SiC substrate exhibit remarkable excitations. The presence of the negative permittivity substrate enables the stimulation of monopolar resonances, which maintain a nearly constant intensity despite variations in the filling fraction of the nanopillars being varied by over an order of magnitude. This occurs along with a broad-band spectral tuning of the modes in excess of 60 cm^{-1}, hence enabling unprecedented performance. This intriguing property is coupled with exceptionally modal high quality factors, with values approaching 300 and strong field localization in the interpillar gap. Moreover, we provide a detailed study of all the modes supported in these SiC resonators, elucidating their intricate spectral dependence on the geometry through both FTIR spectroscopy and numerical simulations. We also confirmed that the coupling among the nanopillars only proceeds through near-field interaction due to their highly subwavelength nature by comparison to aperiodic structures. The coupling mechanisms are further examined in rectangular lattices to probe the relatively uniformities of the near-fields associated with the transverse dipole and monopolar resonances. This work demonstrates that SiC nanoresonators can provide a powerful platform for mid-IR nanophotonics, surface-enhanced spectroscopy, and metamaterials and offer an example for future SPhP-based architectures.

■ METHODS

Fabrication. The samples were designed via electron beam lithography and a standard lift-off process to form Al/Cr hard mask on the semi-insulating 4H-silicon carbide substrates. The substrates were about 350 μm thick. Reactive ion etching was used to fabricate the SiC nanopillars in plasma of equal partial pressure of SF_6 and Ar. A 38 min etching at 150 W results in nanopillars of about 1 μm tall. The protective metal was further removed by wet chemical etching. The aperiodic samples were designed to have the same diameter as the periodic samples of the same diameter. The filling factor is defined by the equation $FF = \pi D^2/4(G + D)^2$, where D is the diameter of the nanopillar and G the interpillar gap.

Measurements. A Bruker Infinion FTIR microscope with a 15× Cassegrain objective was used to collect the reflection signals from the samples. The objective has a weighted-average incident angle of approximately 25°. An aperture of the same size as the nanopillar array ($50 \times 50\ \mu m^2$) was used in all cases. The reflections from the samples were normalized to the reflection from a gold mirror under the same settings.

Simulation. The commercial finite-element method simulation software, COMSOL, was used to calculate the reflection spectra. The 4H-SiC optical constants were determined from ellipsometry. The incident field was directed toward the sample through a port at an angle of 25° in order to approximate the experimental conditions. Floquet boundary conditions were set to mimic the fabricated periodic arrays and perfectly matching layers (PML) for the truncation of the simulation volume.

■ ASSOCIATED CONTENT

Ⓢ Supporting Information

Simulation results showing the interpillar regions, the SEM image of an aperiodic nanopillar array, spectra of samples with D = 0.5 and 0.75 μm, and the effect of metal mask. This material is available free of charge via the Internet at http://pubs.acs.org.

■ AUTHOR INFORMATION

Corresponding Author

*E-mail: s.maier@imperial.ac.uk.

Author Contributions

[†]These authors contributed equally to this work (Y.C. and Y.F.).

Notes

The authors declare no competing financial interest.

■ ACKNOWLEDGMENTS

Y.F., V.G., and S.A.M. were sponsored by the UK Engineering and Physical Sciences Research Council (EPSRC). J.D.C. acknowledges financial support from the NRL Nanoscience Institute (NSI), which is funded by the office of Naval Research. F.J.B. was supported by an ASEE/NRL fellowship. E-beam lithography was performed at the Center for Nanoscale Science and Technology (CNST) at NIST in Gaithersburg MD. T.W.W.M. and T.T. acknowledge funding from the Deutsche Forschungsgemeinschaft (DFG) within SPP-1327 "Sub-100 nm structures for optical and biomedical applications". T.T. acknowledges financial support from the Ministry of Innovation NRW and the German Excellence Initiative.

■ REFERENCES

(1) Giannini, V.; Fernández-Domínguez, A. I.; Sonnefraud, Y.; Roschuk, T.; Fernández-Garciá, R.; Maier, S. A. Controlling Light Localization and Light-Matter Interactions with Nanoplasmonics. *Small* **2010**, *6*, 2498−2507.

(2) West, P. R.; Ishii, S.; Naik, G. V.; Emani, N. K.; Shalaev, V. M.; Boltasseva, A. Searching for Better Plasmonic Materials. *Laser Photonics Rev.* **2010**, *4*, 795−808.

(3) Boltasseva, A.; Atwater, H. A. Low-Loss Plasmonic Metamaterials. *Science* **2011**, *331*, 290−291.

(4) Khurgin, J. B.; Sun, G. Scaling of Losses with Size and Wavelength in Nanoplasmonics and Metamaterials. *Appl. Phys. Lett.* **2011**, *99*, 211106.

(5) Grigorenko, A. N.; Polini, M.; Novoselov, K. S. Graphene Plasmonics. *Nat. Photonics* **2012**, *6*, 749−758.

(6) Hillenbrand, R.; Taubner, T.; Keilmann, F. Phonon-Enhanced Light-Matter Interaction at the Nanometre Scale. *Nature* **2002**, *418*, 159−162.

(7) Caldwell, J. D.; Glembocki, O. J.; Francescato, Y.; Sharac, N.; Giannini, V.; Bezares, F. J.; Long, J. P.; Owrutsky, J. C.; Vurgaftman, I.; Tischler, J. G.; et al. Low-Loss, Extreme Subdiffraction Photon Confinement via Silicon Carbide Localized Surface Phonon Polariton Resonators. *Nano Lett.* **2013**, *13*, 3690−3697.

(8) Wang, T.; Li, P.; Hauer, B.; Chigrin, D. N.; Taubner, T. Optical Properties of Single Infrared Resonant Circular Microcavities for Surface Phonon Polaritons. *Nano Lett.* **2013**, *13*, 5051−5055.

(9) Caldwell, J. D.; Lindsey, L.; Giannini, V.; Vurgaftman, I.; Reinecke, T.; Maier, S. A.; Glembocki, O. J. Low-Loss, Infrared and Terahertz Nanophotonics with Surface Phonon Polaritons. *Nanophotonics* **2014**, submitted for publication.

(10) Caldwell, J. D.; Kretinin, A.; Chen, Y.; Giannini, V.; Fogler, M. M.; Francescato, Y.; Ellis, C. T.; Tischler, J. G.; Woods, C. R.; Giles, A. J. Sub-Diffraction, Volume-Confined Polaritons in the Natural Hyperbolic Material, Hexagonal Boron Nitride. *arXiv:1404.0494 [cond-mat.mtrl-sci], e-prints Arch.* **2014**.

(11) Dai, S.; Fei, Z.; Ma, Q.; Rodin, A. S.; Wagner, M.; McLeod, A. S.; Liu, M. K.; Gannett, W.; Regan, W.; Watanabe, K.; et al. Tunable Phonon Polaritons in Atomically Thin van der Waals Crystals of Boron Nitride. *Science* **2014**, *343*, 1125−1129.

(12) Le Gall, J.; Olivier, M.; Greffet, J.-J. Experimental and Theoretical Study of Reflection and Coherent Thermal Emission by a SiC Grating Supporting a Surface-Phonon Polariton. *Phys. Rev. B* **1997**, *55*, 10105−10114.

(13) Greffet, J.; Carminati, R.; Joulain, K.; Mulet, J.; Mainguy, S.; Chen, Y. Coherent Emission of Light by Thermal Sources. *Nature* **2002**, *416*, 61−64.

(14) Ocelic, N.; Hillenbrand, R. Subwavelength-Scale Tailoring of Surface Phonon Polaritons by Focused Ion-Beam Implantation. *Nat. Mater.* **2004**, *3*, 606−609.

(15) Huber, A.; Ocelic, N.; Kazantsev, D.; Hillenbrand, R. Near-Field Imaging of Mid-Infrared Surface Phonon Polariton Propagation. *Appl. Phys. Lett.* **2005**, *87*, 081103.

(16) Schuller, J. A.; Taubner, T.; Brongersma, M. L. Optical Antenna Thermal Emitters. *Nat. Photonics* **2009**, *3*, 658−661.

(17) Neuner, B., III; Korobkin, D.; Fietz, C.; Carole, D.; Ferro, G.; Shvets, G. Midinfrared Index Sensing of pL-Scale Analytes Based on Surface Phonon Polaritons in Silicon Carbide. *J. Phys. Chem. C* **2010**, *114*, 7489−7491.

(18) Neuner, B., III; Wu, C.; Eyck, G. T.; Sinclair, M.; Brener, I.; Shvets, G. Efficient Infrared Thermal Emitters Based on Low-Albedo Polaritonic *meta*-Surfaces. *Appl. Phys. Lett.* **2013**, *102*, 211111.

(19) Taubner, T.; Korobkin, D.; Urzhumov, Y.; Shvets, G.; Hillenbrand, R. Near-Field Microscopy through a SiC Superlens. *Science* **2006**, *313*, 1595.

(20) Korobkin, D.; Urzhumov, Y.; Neuner, B., III.; Zorman, C.; Zhang, Z.; Mayergoyz, I.; Shvets, G. Mid-Infrared Metamaterial Based on Perforated SiC Membrane: Engineering Optical Response Using Surface Phonon Polaritons. *Appl. Phys. A: Mater. Sci. Process.* **2007**, *88*, 605−609.

(21) Schuller, J. A.; Zia, R.; Taubner, T.; Brongersma, M. L. Dielectric Metamaterials Based on Electric and Magnetic Resonances of Silicon Carbide Particles. *Phys. Rev. Lett.* **2007**, 99.

(22) Auguie, B.; Barnes, W. L. Collective Resonances in Gold Nanoparticle Arrays. *Phys. Rev. Lett.* **2008**, *101*.

(23) Liu, Z.; Boltasseva, A.; Pedersen, R. H.; Bakker, R.; Kildishev, A. V.; Drachev, V. P.; Shalaev, V. M. Plasmonic Nanoantenna Arrays for the Visible. *Metamaterials* **2008**, *2*, 45−51.

(24) Adato, R.; Yanik, A. A.; Amsden, J. J.; Kaplan, D. L.; Omenetto, F. G.; Hong, M. K.; Erramilli, S.; Altug, H. Ultra-Sensitive Vibrational Spectroscopy of Protein Monolayers with Plasmonic Nanoantenna Arrays. *Proc. Natl. Acad. Sci. U.S.A.* **2009**, *106*, 19227−19232.

(25) Auguie, B.; Bendana, X. M.; Barnes, W. L.; Garcia de Abajo, F. J. Diffractive Arrays of Gold Nanoparticles near an Interface: Critical Role of the Substrate. *Phys. Rev. B* **2010**, *82*.

(26) Kullock, R.; Grafstroem, S.; Evans, P. R.; Pollard, R. J.; Eng, L. M. Metallic Nanorod Arrays: Negative Refraction and Optical Properties Explained by Retarded Dipolar Interactions. *J. Opt. Soc. Am. B* **2010**, *27*, 1819−1827.

(27) Caldwell, J. D.; Glembocki, O.; Bezares, F. J.; Bassim, N. D.; Rendell, R. W.; Feygelson, M.; Ukaegbu, M.; Kasica, R.; Shirey, L.; Hosten, C. Plasmonic Nanopillar Arrays for Large-Area, High-Enhancement Surface-Enhanced Raman Scattering Sensors. *ACS Nano* **2011**, *5*, 4046−4055.

(28) Simpkins, B. S.; Long, J. P.; Glembocki, O. J.; Guo, J.; Caldwell, J. D.; Owrutsky, J. C. Pitch-Dependent Resonances and near-Field Coupling in Infrared Nanoantenna Arrays. *Opt. Express* **2012**, *20*, 27725−27739.

(29) Mutschke, H.; Andersen, A. C.; Clément, D.; Henning, T.; Peiter, G. Infrared Properties of SiC Particles. *Astron. Astrophys.* **1999**, *345*, 187−202.

(30) Anderson, M. Surface Enhanced Infrared Absorption by Coupling Phonon and Plasma Resonance. *Appl. Phys. Lett.* **2005**, *87*.

(31) Rockstuhl, C.; Salt, M. G.; Herzig, H. P. Analysis of the Phonon-Polariton Response of Silicon Carbide Microparticles and Nanoparticles by Use of the Boundary Element Method. *J. Opt. Soc. Am. B* **2005**, *22*, 481−487.

(32) Taminiau, T. H.; Moerland, R. J.; Segerink, F. B.; Kuipers, L.; van Hulst, N. F. $\lambda/4$ Resonance of an Optical Monopole Antenna Probed by Single Molecule Fluorescence. *Nano Lett.* **2007**, *7*, 28−33.

(33) Çetin, A. E.; Yanik, A. A.; Yilmaz, C.; Somu, S.; Busnaina, A.; Altug, H. Monopole Antenna Arrays for Optical Trapping, Spectroscopy, And Sensing. *Appl. Phys. Lett.* **2011**, *98*, 111110.

(34) Tiwald, T.; Woollam, J.; Zollner, S.; Christiansen, J.; Gregory, R.; Wetteroth, T.; Wilson, S.; Powell, A. Carrier Concentration and Lattice Absorption in Bulk and Epitaxial Silicon Carbide Determined Using Infrared Ellipsometry. *Phys. Rev. B* **1999**, *60*, 11464−11474.

(35) Adachi, S. *Optical Properties of Crystalline and Amorphous Semiconductors: Materials and Fundamental Principles*; Springer: New York, U.S.A., 1999; pp 33−61.

(36) Bohren, C. F.; Huffman, D. R. *Absorption and Scattering of Light by Small Particles*; Wiley-VCH: Weinheim, Germany, 1998; pp 241−244.

(37) Reininghaus, M.; Wortmann, D.; Cao, Z.; Hoffmann, J. M.; Taubner, T. Fabrication and Spectral Tuning of Standing Gold Infrared Antennas Using Single fs-Laser Pulses. *Opt. Express* **2013**, *21*, 32176−32183.

(38) Acar, H.; Coenen, T.; Polman, A.; Kuipers, L. K. Dispersive Ground Plane Core−Shell Type Optical Monopole Antennas Fabricated with Electron Beam Induced Deposition. *ACS Nano* **2012**, *6*, 8226−8232.

(39) Myroshnychenko, V.; Rodriguez-Fernandez, J.; Pastoriza-Santos, I.; Funston, A. M.; Novo, C.; Mulvaney, P.; Liz-Marzan, L. M.; Garcia de Abajo, F. J. Modelling the Optical Response of Gold Nanoparticles. *Chem. Soc. Rev.* **2008**, *37*, 1792−1805.

(40) Bohren, C. F.; Huffman, D. R. *Absorption and Scattering of Light by Small Particles*; Wiley-VCH: Weinheim, Germany, 1998; pp 325−380.

(41) Halas, N. J.; Lal, S.; Chang, W.-S.; Link, S.; Nordlander, P. Plasmons in Strongly Coupled Metallic Nanostructures. *Chem. Rev.* **2011**, *111*, 3913−3961.

(42) Alonso-Gonzalez, P.; Schnell, M.; Sarriugarte, P.; Sobhani, H.; Wu, C.; Arju, N.; Khanikaev, A.; Golmar, F.; Albella, P.; Arzubiaga, L.; et al. Real-Space Mapping of Fano Interference in Plasmonic Metamolecules. *Nano Lett.* **2011**, *11*, 3922−3926.